Published in final edited form as:

J Drug Deliv Sci Technol. 2018 February ; 43: 453–460. doi:10.1016/j.jddst.2017.11.013.

Chitosan-Mangafodipir nanoparticles designed for intranasal delivery of siRNA and DNA to brain

Juan Sanchez-Ramos[a,*], **Shijie Song**[a], **Xiaoyuan Kong**[a], **Parastou Foroutan**[b], **Gary Martinez**[b], **William Dominguez-Viqueria**[b], **Shyam Mohapatra**[c], **Subhra Mohapatra**[d], **Reka A. Haraszti**[e], **Anastasia Khvorova**[e], **Neil Aronin**[f], and **Vasyl Sava**[a]

[a]Department of Neurology, University of South Florida, Tampa, FL, USA

[b]Moffit Cancer Center and Research Institute, Tampa, FL, USA

[c]Nanomedicine Research Center, Tampa, FL, USA

[d]Department of Molecular Medicine, Tampa, FL, USA

[e]RNA Therapeutics Institute, University of Massachusetts Medical School, Worcester, MA, USA

[f]Department of Medicine, University of Massachusetts Medical School, Worcester, MA, USA

Abstract

The overall objective of the present research was to develop a nanocarrier system for non-invasive delivery to brain of molecules useful for gene therapy. Manganese-containing nanoparticles (mNPs) carrying *anti*-eGFP siRNA were tested in cell cultures of eGFP-expressing cell line of mouse fibroblasts (NIH3T3). The optimal mNPs were then tested *in vivo* in mice. Following intranasal instillation, mNPs were visualized by 7T MRI throughout brain at 24 and 48 hrs. mNPs were effective in significantly reducing GFP mRNA expression in Tg GFP+ mice in olfactory bulb, striatum, hippocampus and cortex. Intranasal instillation of mNPS loaded with dsDNA encoding RFP also resulted in expression of the RFP in multiple brain regions. In conclusion, mNPs carrying siRNA, or dsDNA were capable of delivering the payload from nose to brain. This approach for delivery of gene therapies to humans, if successful, will have a significant impact on disease-modifying therapeutics of neurodegenerative diseases.

Keywords

Intranasal route; Nanocarrier; Gene silencing; Small animal MRI

1. Background

Gene therapy is a promising molecular approach that can impact disease progression by modulating gene expression, either by suppressing deleterious genes or increasing

[*]Corresponding author. Dept of Neurology, University of South Florida, 13220 Laurel Drive, Tampa, FL 33612, USA. jsramos@health.usf.edu (J. Sanchez-Ramos).

Conflicts of interest

Some of the authors (JS-R, VS, SS, SM, SM) are named inventors on an international patent application related to “The Use Of Manganese-Containing Nanoparticles For Delivery Of Gene-Modifying Molecules To Brain”.

expression of beneficial genes. Gene expression can be silenced with anti-sense oligonucleotides (ASO) or small interfering RNA (siRNA). *In vivo* delivery of siRNA or ASO has been shown to be effective in animal models of Alzheimer's disease (AD), amyotrophic lateral sclerosis (ALS), Huntington's disease (HD), spinocerebellar ataxia (SCA), anxiety, depression, neuropathic pain, encephalitis and glioblastoma [1].

Another aspect of gene therapy is directed towards increasing gene expression of enzymes involved in biosynthesis of neurotransmitters or biosynthesis of neurotrophic factors. A total of 10 clinical trials of gene therapy for patients with Parkinson's Disease (PD) have been undertaken [2]. Many of the studies report improvements in some aspects of motor function, but none has advanced beyond Phase II [3–8].

A major obstacle to fulfilling the therapeutic promise of gene therapy is the requirement for an invasive delivery system (stereotaxic injection of viral vectors or infusion of ASO directly into brain or intrathecal space) [9–11]. For diseases like HD and PD that gradually encompass the entire central nervous system (CNS), repeated injections of the agent (vector encoding DNA, siRNA or ASO) into multiple brain regions over the course of the illness make it unfeasible and unacceptable. Chronic infusion of siRNA or ASO directly into brain parenchyma or into the cerebrospinal fluid via intrathecal administration using pumps is a viable approach but is liable to complications associated with neurosurgical procedures in the atrophic HD brain (increased risk of hemorrhage, infection). Another problem with the current state of the art is the reliance on viral vectors (adeno-associated viruses or lentiviruses) to deliver the gene of interest. Applying these vectors to humans carries a certain amount of risk that can be bypassed by using other vehicles and routes for gene delivery into brain. These obstacles to delivery of *anti*-htt siRNA has led to the present research project which explores the intranasal administration of siRNA or DNA packaged in manganese-containing chitosan-matrix nanoparticles (mNPs) that can be delivered non-invasively to brain. This delivery system evolved from abundant evidence that manganese and relatively large aggregates of manganese oxide particles are actively transported directly into brain by the olfactory and trigeminal nerves [12,13] or via the perineural channels that envelop olfactory and trigeminal nerve axons [14].

The overall goal of the research presented here was to develop a nanocarrier system for delivery into brain of gene-modulating molecules that otherwise could not access the CNS. The first specific goal was to optimize the design of nanoparticles (NP) carrying siRNA by testing their efficacy in silencing a target gene, green fluorescent protein (GFP) in a cell culture system that expresses GFP. The second specific goal was to demonstrate that Mn-containing nanocarriers bearing siRNA can be visualized *in vivo* by MRI and tracked over time as the mNPs are distributed from olfactory bulb to other regions of brain. The third objective was to test if intranasal instillation of mNPs loaded with *anti*-GFP siRNA would decrease expression of GFP in Tg "green mice". The fourth objective was to determine if mNPS loaded with dsDNA encoding red fluorescent protein (RFP) would be transported from nose to brain and result in expression of the payload in various brain regions.

2. Methods

Animals

All *in vivo* animal experiments were performed in accordance with the guidelines of the University of South Florida IACUC committee. Transgenic “green mice” (C57BL/6-Tg (ACTbEGFP)1Osb/J were purchased from JAX Labs, Inc; Bar Harbor, Maine, USA). These mice, which exhibit GFP+ neurons were utilized to measure the extent of GFP silencing. Normal C57Bl6J mice were used when the nanocarrier payload was dsDNA encoding red fluorescent protein (RFP) or Cy3-hsiRNA.

Fabrication of NPs

Low molecular weight chitosan (Sigma-Aldrich, Inc. St. Louis, MO) was dissolved in 1–2 mg/ml in 0.5% aqueous acetic acid solution at ambient temperature with continuous agitation for 6 h following filtration through 0.2 μm filter. Mangafodipir (MFDP) solution (0.1–4 mg/ml) was prepared in deionized water. The optimal conditions required for the formation of chitosan/MFDP coacervates (spherical colloidal droplets held together by electrostatic attractive forces) were established by ranging volumetric mixing ratios chitosan/MFDP from 0.5 to 5. Dynamic Light Scattering (DLS) measurements were carried out for adjustment of nanoparticle preparation. Nanoparticles were isolated by centrifugation at 10,000 rpm for 30 min. The coacervates in the pellet were collected and the supernatant was discarded. The separation procedure was repeated three times. For incorporation of siRNA or DNA into chitosan–MFDP nanoparticles, 10–20 μM of oligonucleotide was added to 0.1–0.2% solution of chitosan allowing binding for 3 hr. Later on, the MFDP solution (1–10 mg/ml) was added drop-wise under continuous magnetic stirring at room temperature. The preparations were kept at room temperature for 1 hr before separation procedure.

Characterization of the NPs

The hydrodynamic particle diameters of the NPs and the size distributions were measured using Dynamic Light Scattering Particle Size Distribution Analyzer LB-500 (HORIBA INSTRUMENTS INC., Irvine, CA, U.S.A.) equipped with 5-mW laser source generating wavelength of 650 nm. Processing the optical signal with digital auto-correlator allowed determination of the equivalent spherical particle size based on the Stokes–Einstein equation in range from 3 nm to 6000 nm. For size determination, 3 ml of each sample was placed in a disposable cuvette with interior length 10 × 10 mm. The instrument maintained temperature stabilization during all measurements. The samples were analyzed at 25 °C. Mean diameter ± SEM (n = 6 replications) was measured for each mNP carrying distinct nucleic acid payloads (See Table 1). The system was calibrated using standard polystyrene beads (Polysciences, Warrington, PA) with a mean hydrodynamic diameter of 100 nm.

For scanning electron microscopy, a 200 μL sample was spread onto carbon adhesive tape attached to a standard aluminum specimen stab and allowed to air dry. Samples were examined uncoated with a JEOL LSM-6490LV at 12–14 kV. Several images were obtained for each sample, ensuring reproducibility.

Cell Culture studies

mNPs containing *anti-GFP* siRNA in a chitosan polymer matrix were tested in a cell culture system of eGFP-expressing mouse fibroblast cultures (NIH3T line from Cell Biolabs, Inc., San Diego, CA, USA). The mNPs were synthesized using low molecular weight chitosan (average = 89 kDa), a manganese chelate (MFDP) and siRNA or plasmid dsDNA as previously described [12]. The amount of the Mn-chelate added was 58 μM, with an estimated 470 Mn molecules per nanoparticle. In one of the MR studies, a lower concentration of Mn was also used (235 Mn molecules per NP) to determine if the NPs could still be visualized on the T_1 images. The estimated number of chitosan molecules per NP was 36 and the number of siRNA molecules loaded per NP was approximately 81. The number of chitosan molecules appears to be small, but that is because of the polymeric nature of chitosan. Given that the chitosan has an average molecular weight of 89,000 DA and one molecule of chitosan consists of 494 D-glucosamine units, there are approximately 17784 units of chitosan in the NP scaffold.

mNPs, loaded with siRNA against eGFP were compared to the effects of Lipofectamine RNAi-MAX transfection reagent (ThermoFisher Scientific) in silencing eGFP in eGFP-expressing fibroblast cells (NIH3T3). Silencing efficacy and cytotoxicity was assessed using fluorescence plate reader and subsequently confirmed using Fluorescence Activated Cell Sorting (FACS). (See Supplemental material for FACS results). Transfection of NIH3T3/GFP cells was performed in 24-well plate exposed to chitosan NPs or Lipofectamine loaded with *anti*-eGFP siRNA. Experimental conditions were as follows: Initial cell density = 30,000/well; siRNA concentration = 10–40 nM; Lipofectamine concentration = 2 μL/well.

Payloads packaged into mNPs

Stealth™ RNAi GFP siRNA (Invitrogen, CA) was used to fabricate mNP for *in vivo* RNA interference experiments.

Plasmid dsDNA encoding Cherry Red RFP was purchased from Addgene - pQCXIB CMV/TO DsRed2 (Cambridge, MA, USA). Hydrophobically modified Cy3-tagged siRNA (hsiRNA) directed against the huntingtin gene (htt) mRNA was prepared in the Khvorova lab using methods previously described [15] (See Supplemental material).

Magnetic Resonance Imaging (MRI) was performed using a 7-T horizontal bore Scanner with a Bruker Biospec AV3HD and a 2-element cryoprobe. Each mouse was imaged individually. Prior to imaging, mice were placed in an induction chamber and anesthetized using 1% isoflurane for 5 min. Upon complete anesthetization, mice were immobilized in a custom-built insertion device equipped with a respiratory pillow and rectal probe for monitoring of respiratory functions and body temperature, respectively. While inside the magnet, the mice continuously received isoflurane and heated air, and all physiological functions were controlled with SAII monitoring and gating systems (Small Animal Instruments, Inc.).

For anatomical reference and image segmentation a TurboRare sequence was used to image in coronal and axial images of the brain with repetition time (TR) = 2427 ms, echo time

(TE) = 72 ms, Matrix = 256 × 256, Field Of View = 20 × 20 mm and 11 slices with 0.4 mm thickness. Similarly T1-weighted Spin-Echo datasets were acquired with repetition time (TR) = 264 ms, echo time (TE) = 11 ms. The spatial resolution was thus 78 × 78 × 400 μm. MRI was performed at 24, and 48 h post intranasal administration. Mouse number 1 was not administered with mNPs and imaged at the same time as all the others as control. Image reconstruction and quantitative signal analysis was performed using in-house written scripts in Matlab (Mathworks Inc.).

Measurement of Cy3-tagged hsiRNA in brain regions with HPLC and fluorescence detector: A special extraction buffer was developed for this purpose (See Supplemental Material). The extraction buffer contained the following components: 25 mM Tris-HCl, pH 7.4; 20 mM NaCl; 1 mM EDTA; and 0.5% zwitterionic detergent EMPIGEN allowing direct injection of the siRNA extract into HPLC column for analysis avoiding irreversible binding detergent to the column. Optical density was recorded at 550 nm and fluorescent signal for Cy-3 tag was obtained by using 550 nm excitation and 570 nm emission wavelengths.

Analysis was performed on Perking Elmer series 200 HPLC with auto sampler and both UV and Fluorescence detector. Binary gradient pump delivers two eluents A and B programmed to create gradient in anion-exchange DNAPac PA100 oligonucleotide column (Thermofisher, Rockford, IL) suitable for elution of siRNA. **Eluent A**: 50 mM Tris Buffer, 2 mM EDTA and 50% acetonitrile (pH 8.0).

Eluent B: 50 mM Tris Buffer, 2 mM EDTA; 2.6 M NaClO4 and 50% acetonitrile (pH 8.0). The concentrations of nasally administered hsiRNA measured in each brain region was expressed as pg/ml and as percentage of nasal dose in each brain region.

Quantitative rtPCR measurements of GFP silencing *in vivo*

Stealth™ RNAi GFP siRNA (Invitrogen, CA) was used to fabricate mNP for *in vivo* RNA interference experiments. Main constituents comprising chitosan (CS), siRNA (RNAi) and manganese chelate participated in formation of 120 ± 15 nm mNP were presented by following ratios: RNAi/Mn/CS = 2/12/1.

Each animal received 40 μL of mNP suspension contained 0.38 nmoles of GFP siRNA in each nostril during 40 min of instillation session under isofluran anesthesia. Animals were sacrificed in 48 hr after treatment and brain tissue was dissected for analysis including RNA extraction, reverse transcription and evaluation of GFP expression by quantitative real PCR.

Extraction of GFP mRNA dissected brain tissue was carried out with RNeasy Plus Mini Kit (Quiagen, CA) according to manufacturer protocol. Approximately 30 mg of brain tissue was taken for each test yielding 15–30 μg total RNA with average concentration of 1 μg/μl. The following reverse transcription reaction was carried out with Quiagen's Quanti Tect kit and the quantitative real time PCR was performed on ViiA7 instrument (Applied Biosystems) with QuantiTect SYBR Green PCR Kit (Quiagen, CA) as instructed by manufacturer protocol.

The following primers were utilized for amplification of GFP and actin (ACT) as internal standard:

GFP-F: 5′-tggtgagcaagggcgaggag-3′

GFP-R: 5′-gggggtgttctgctggtagt-3;

ACT-F: 5′-ggctgtattcccctccatcg-3′

ACT-R: 5′-ccagttggtaacaatgccatgt-3′

Analysis of relative GFP expression was performed by using 2-delta-delta-*C*T method as previously described [16].

Quantitative rtPCR based measurements of pmCherry concentration in brain tissue: To fabricate mNP for *in vivo* delivery of oligonucleotides we used pmCherry-N1 (Clontech laboratories, CA). Main constituents comprising chitosan (CS), plasmid (PL) and manganese chelate participated in formation of 120 ± 15 nm mNP were presented by following molecular ratios: CS/Mn/PL = 25/321/1.

Each animal received 40 μL of mNP suspension contained 8.9 μg or 5.6 pmol of pmCherry in each nostril during 40 min of instillation session under isofluran anesthesia. Animals were sacrificed in 48 hr after treatment and brain tissue was dissected for analysis consisted of DNA extraction and assessment of plasmid content by quantitative real time PCR. DNeasy kit (Qiagen, CA) was employed for DNA extraction from dissected brain regions. Procedure was performed according to manufacturer recommendation. Approximately 25 mg of brain tissue was taken for each test yielding 10–20 μg of total DNA with average concentration of 100 μg/ml 2xQuanti Tect SYBR green Master Mix was used for quantitative PCR amplification of extracted plasmid DNA. The following primers were obtained from Invitrogen:

F: 5′-cgacgctgaggtcaagaccacc -3′

R: 5′-ctcgttgtgggaggtgatgtccaac-3′

Concentration of plasmid in brain tissue was calculated from Standard Curve obtained by PCR amplification of serially diluted pure mCherry plasmid.

3. Statistical analysis

a. Results from cell culture studies are expressed as mean ± SEM (n = 8 samples per treatment). Two-way ANOVA (treatment and time factors) followed by correction for multiple comparisons (Tukey multiple comparisons test) was performed using GraphPad Prism v6 (GraphPad Software, La Jolla California USA, www.graphpad.com)

b. MRI data are expressed as mean signal ± SEM. One-way ANOVA was performed using Matlab Statistics Toolbox (Mathworks, Inc., Natick, MA). A confidence interval of 95% was chosen and statistical significance was pre-determined at $p < 0.05$.

c. GFP expression in brain regions is expressed as mean RQ-1 (+/−SEM; n = 4–6). A one sample *t*-test comparing mean RQ-1 to untreated control in each brain region was performed using GraphPad Prism v6 (La Jolla, CA).

d. Data from the measurement of hsiRNA levels in brain regions over time was expressed as mean concentration (ng/g tissue) +/− SEM (n = 4–6 per brain region)

e. Data from cherry red dsDNA expression following administration of NP-dsDNA is expressed as mean DNA concentration ± SEM (n = 4 per brain region).

4. Results

Nanoparticles were fabricated by coacervation of nucleic acids (siRNA or DNA) with chitosan and Mangafodipir (MFDP) serving as the intermolecular cross-linker for the chitosan polymer. The effect of fabrication conditions on the physical properties was examined by dynamic light scattering (DLS) and scanning electron microscopy (SEM). The nanoparticles formed only within a certain range of chitosan, DNA/RNA and MFDP concentrations. SEM of the NPs revealed a core–shell structure for nanoparticles with a median dry diameter of 100 nm (range of 90–114 nm) (Fig. 1). All experiments described here utilized mNPs within this size range.

Incubation of the NIHT3 cells with mNPs containing *anti*-GFP siRNA resulted in statistically significant down regulation of GFP expression. The overall reductions in GFP fluorescence at both 48 and 72 hr can be seen visually with fluorescence microscopy and measured by fluorescence at 520 nm (Fig. 2). Although there was no significant difference between effects of mNP and lipofectamine at 72 hr (77% reduction with mNP and 84% reduction with lipofectamine), the mNPs were found less effective at 48 hr than the lipofectamine. This suggests a slower release of *anti*-GFP content from mNPs.

Lipofectamine is broadly used as the reference standard for evaluation of transfection efficacy with new nanoparticles. This comparison with lipofectamine is not especially useful in predicting *in vivo* outcomes especially with nanoparticles that slowly release the payload. More likely, fast release will exhaust nanoparticle capacity to deliver content to the intended targets deeper in brain.

Another important feature of the novel mNPs is their low toxicity. Fluorescence activated cell sorting (FACS) was used to enumerate ethidium + cells as an index of toxicity as well as to count GFP+ cells (See Supplementary Material, Fig S-5). The percentage of total cells that were ethidium+ (“dead” cells) after 72 h was 3.89% in lipofectamine-treated cultures compared to 2.15% in mNP-treated cultures. These results indicate that presence of Mn in nanoparticles in amounts used for fabrication was not toxic and did not impede gene silencing.

In vivo studies revealed accumulation of mNPs in olfactory bulb and other brain regions after intranasal installation. MR imaging of anesthetized mice 24 and 48 hr after intranasal instillation of mNPs carrying *anti*-GFP siRNA showed accumulation of NPs in various brain regions, indicated by increased manganese signal intensity in T_1-weighted images. The Mn

signal was quantified in 4 brain regions using parcellation software. The analyzed regions (olfactory bulb, hippocampus, cerebral cortex and corpus striatum) all exhibited significant increases in Mn signal, peaking at 24 hr (Fig. 3E–F). It is possible that peak Mn signal might have been higher in olfactory bulb if scanning had been done earlier than 24 hr. The greatest change in Mn signal was measured in the cerebral cortex, where the signal increased to a mean of 97 ± 17% of baseline at 24 hr and declined to 48.6 ± 17.4% after 48 hr. The peak changes in Mn signal in other regions were somewhat less but comparable to the cerebral cortex (hippocampus = 89.1 ± 19.7%; striatum = 77.3 ± 14.4% olfactory bulb = 68.6 ± 19.4%; of baseline). These results replicate the time course of Mn signal obtained from an earlier experiment conducted in an older small bore MRI system before the updraded equipment used to generate the present MRI data. That earlier study used a different set of mice and explored NPs with two concentrations of Mn (see Supplementary Material, Fig S-6). All four brain regions exhibited peak Mn signal at 24 hrs followed by a dropoff by 48 hrs. In that earlier experiment, olfactory bulb had the highest Mn signal at 24 hrs.

After completion of the MR scans at 48 h, mice were euthanized and 4 brain regions were dissected and processed for RT-PCR of GFP mRNA expression. GFP mRNA levels were significantly decreased in all brain regions analyzed (Fig. 4). All four regions exhibited at least a 50% decrease in GFP mRNA expression. No attempt was made to quantify fluorescence intensity in various brain regions because GFP fluorescence is cell-type specific and exhibits various degrees of fluorescence intensity within specific cells in this Tg “green mouse. (see Supplementary Material Figs. S–7).

To determine the actual concentrations of the siRNA carried by the NPs, we utilized a novel method to measure hsiRNA tagged with the fluorescent marker Cy3, in each of four brain regions using HPLC with fluorescence detector (Fig. 5). This Cy3-hsiRNA was designed to a) allow quantitative measurement of its levels in brain tissue over time and b) to silence the Huntington’s Disease (htt) gene [15] (See Supplementary Material describing sequence of hsiRNA). Future studies are planned to test the *anti*-htt mNPs-Cy3-hsiRNA in a mouse model of HD. In the first 12 hrs, the highest levels of hsiRNA were found in olfactory bulb and hippocampus with very low levels found in cortex and striatum at 12 hrs. By 48 hrs after administration, levels in cerebral cortex and striatum were much higher than olfactory bulb and hippocampus. Of the total amount of hsiRNA administered intranasally, approximately 0.7% of that dose was distributed to cortex, striatum and olfactory bulb (Fig. 5B).

To determine the extent to which genes can be expressed in various brain regions following intranasal administration, dsDNA encoding RFP was packaged into mNPs. Forty-eight hours after intranasal instillation, RFP was visualized in olfactory bulb, striatum, cortex and hippocampus (Fig. 6). The fluorescence signal of the RFP expressed gene was co-expressed in tyrosine hydroxylase (TH+) neurons in the zona glomerulosa of the olfactory bulb (Fig. 6A). RFP was also expressed in other cell types, not identified at this time. In the ventral striatum co-expression of RFP within neurons (NeuN + cells) revealed the perinuclear pattern of its expression (Fig. 6C). Striatal RFP DNA levels were higher than other brain regions at 48 hrs after intranasal administration of the nanoparticles (Fig. 6D).

5. Discussion

The intranasal route of drug delivery has traditionally been used to administer small, lipophilic drugs that are rapidly absorbed into the capillaries of the nasal epithelium, resulting in rapid onset of CNS actions. Many neurotherapeutic agents, especially polynucleotides and proteins, do not readily cross the blood-brain barrier and cannot survive intact in the gut or blood. Hence, gene therapy for brain disorders has required direct neurosurgical microinjection or infusion into brain or cerebrospinal fluid. However, recent research has demonstrated direct nose-to-brain delivery of relatively large molecules, including neurotrophins (NGF and insulin-like growth factor [IGF]-1), neuropeptides, cytokines (interferon β-1b and erythropoietin as well as polynucleotides (DNA plasmids and genes) [17–24]. In a most recent example, compacted DNA nanoparticles (encoding a reporter gene, eGFP) were successfully delivered from nose to brain in rats without the need for viral vectors. [24] eGFP protein expression was observed 2 days after intranasal delivery and were found throughout the rostral-caudal axis of the brain.

The present report demonstrates a novel manganese-chelate nano-carrier system for direct nose-to-brain delivery of siRNA and DNA. Inclusion of Mn in the nanocarrier structure was shown to be useful in tracking the distribution of the NPs *in vivo*. In addition, Mn content of the nanocarrier did not impede the functional activity of siRNA or the expression of DNA. eGFP mRNA expression was decreased by at least 50% in four brain regions that also exhibited significantly increased Mn signal in T_1-weighted MR images. mNPs loaded with dsDNA encoding RFP was expressed in corpus striatum and other regions following intranasal administration. Hence, this novel nanocarrier system was effective in delivering nucleic acid payloads that exhibited the expected activity in brain tissue.

There are three potential nose-to-brain routes that bypass the blood-brain-barrier [14]: 1) Direct uptake into olfactory or trigmeninal nerve terminals with axonal transport to the olfactory bulb and pons, respectively, as has been shown with manganese particles alone; 2) Transport via perineural spaces to the cerebrospinal fluid followed by distribution along the sub-arachnoid space where NPs are carried along by bulk flow; 3) Transport along perivascular channels. This last route was the most likely mechanism by which compacted DNA was transported from nose to the entire neuraxis [24].

The direct uptake of NPs by olfactory sensory neurons involves endocytosis, which can be either clathrin receptor-mediated or receptor-independent macropinocytosis [25]. We hypothesize that the divalent metal transporter may be important in the early endosomal processing of the NPs during which the chitosan is metabolized, Mn++ ion is transported out of the endosome and siRNA escapes into cytoplasm. Furthermore, it is hypothesized that late endosomes carry the residual mNPs to the Golgi apparatus and from there, small exosomes can be extruded by exocytosis into the extracellular milieu. Presumably other cells take up the mNPs and repeat the process, resulting in dissemination of the NPs to other regions of brain.

A potential pitfall inherent in this study is that cellular processing of the NP in the olfactory bulb (or other brain regions) will liberate Mn allowing it to disseminate throughout the brain

independent of its payload (plasmid DNA or siRNA). In fact, free Mn++ ion, released from its chelate Mangafodipir, is responsible for MR contrast on T1-weighted imaging [26]. Relying on distribution of the Mn signal alone cannot provide information on how well the plasmid DNA or siRNA is transported along with the Mn to those regions. Therefore, the actual concentrations of the siRNA in each brain region needs to be measured, as was done for the Cy3-tagged hsiRNA in the present report.

Mn delivered chronically at high concentrations can be neurotoxic [27–30]. However, Mn is cleared very efficiently from brain and body by homeostatic mechanisms, providing the liver is healthy [31,32]. Moreover, the amount of Mn included in the NPs (58 μM) was 5 fold lower than previously reported cytotoxic concentrations. Studies of Mn toxicity in PC12 cells have shown 50% cell death at 48 h when 300 μM was added to the cultures [33]. Other reports have shown concentrations of $MnCl_2$ from 50 to 500 μM added to PC12 cells were minimally toxic, unless melanin was added to the mix [34]. As shown in the present report, addition of manganese-containing nanocarriers of siRNA directly to cells *in vitro* was not any more toxic than lipofectamine delivery of siRNA, with dead cells ranging from 2 to 4% of total cells in culture.

The greatest advantage of the nanocarrier approach described here will be the ability to dose patients simply, non-invasively and chronically via intra-nasal administration of nanocarriers of gene-silencing agents or other large therapeutic molecules. The nanocarriers will have their greatest impact on neurodegenerative disorders but will also be advantageous for slowing normal aging processes in brain because of the ability to intermittently deliver growth factors packaged in the NPs. The intranasal delivery of nanocarriers will have a widespread and dramatic impact in the therapeutics of brain disorders and normal aging.

Supplementary Material

Refer to Web version on PubMed Central for supplementary material.

Acknowledgments

This work was supported by the National Institutes of Health: R01 NS095563 (09/01/2015 to 08/31/2020) to JSR, University of South Florida and NIH instrumentation grant S10 OD020012 to AV, University of Massachusetts, Worcester.

References

1. Sah DW. Therapeutic potential of RNA interference for neurological disorders. Life Sci. 2006; 79(19):1773–1780. [PubMed: 16815477]
2. Bartus RT, Weinberg MS, Samulski RJ. Parkinson's disease gene therapy: success by design meets failure by efficacy. Mol Ther. 2014; 22(3):487–497. [PubMed: 24356252]
3. Kaplitt MG, Feigin A, Tang C, Fitzsimons HL, Mattis P, Lawlor PA, et al. Safety and tolerability of gene therapy with an adeno-associated virus (AAV) borne GAD gene for Parkinson's disease: an open label, phase I trial. Lancet. 2007; 369(9579):2097–2105. [PubMed: 17586305]
4. Christine CW, Starr PA, Larson PS, Eberling JL, Jagust WJ, Hawkins RA, et al. Safety and tolerability of putaminal AADC gene therapy for Parkinson disease. Neurology. 2009; 73(20):1662–1669. [PubMed: 19828868]

5. Marks WJ Jr, Bartus RT, Siffert J, Davis CS, Lozano A, Boulis N, et al. Gene delivery of AAV2-neurturin for Parkinson's disease: a double-blind, randomised, controlled trial. Lancet Neurol. 2010; 9(12):1164–1172. [PubMed: 20970382]
6. Mittermeyer G, Christine CW, Rosenbluth KH, Baker SL, Starr P, Larson P, et al. Long-term evaluation of a phase 1 study of AADC gene therapy for Parkinson's disease. Hum Gene Ther. 2012; 23(4):377–381. [PubMed: 22424171]
7. Bartus RT, Baumann TL, Brown L, Kruegel BR, Ostrove JM, Herzog CD. Advancing neurotrophic factors as treatments for age-related neurodegenerative diseases: developing and demonstrating "clinical proof-of-concept" for AAV-neurturin (CERE-120) in Parkinson's disease. Neurobiol Aging. 2013; 34(1):35–61. [PubMed: 22926166]
8. Palfi S, Gurruchaga JM, Ralph GS, Lepetit H, Lavisse S, Buttery PC, et al. Long-term safety and tolerability of ProSavin, a lentiviral vector-based gene therapy for Parkinson's disease: a dose escalation, open-label, phase 1/2 trial. Lancet. 2014; 383(9923):1138–1146. [PubMed: 24412048]
9. Dreyer JL. Lentiviral vector-mediated gene transfer and RNA silencing technology in neuronal dysfunctions. Mol Biotechnol. 2011; 47(2):169–187. [PubMed: 20862616]
10. Farah MH. RNAi silencing in mouse models of neurodegenerative diseases. Curr Drug Deliv. 2007; 4(2):161–167. [PubMed: 17456035]
11. Kordasiewicz HB, Stanek LM, Wancewicz EV, Mazur C, McAlonis MM, Pytel KA, et al. Sustained therapeutic reversal of Huntington's disease by transient repression of huntingtin synthesis. Neuron. 2012; 74(6):1031–1044. [PubMed: 22726834]
12. Dorman DC, Brenneman KA, McElveen AM, Lynch SE, Roberts KC, Wong BA. Olfactory transport: a direct route of delivery of inhaled manganese phosphate to the rat brain. J Toxicol Environ Health. 2002; 65(20):1493–1511.
13. Gianutsos G, Morrow GR, Morris JB. Accumulation of manganese in rat brain following intranasal administration. Fundam Appl Toxicol. 1997; 37(2):102–105. [PubMed: 9242582]
14. Dhuria SV, Hanson LR, Frey WH 2nd. Intranasal delivery to the central nervous system: mechanisms and experimental considerations. J Pharm Sci. 2010; 99(4):1654–1673. [PubMed: 19877171]
15. Alterman JF, Hall LM, Coles AH, Hassler MR, Didiot MC, Chase K, et al. Hydrophobically modified siRNAs silence huntingtin mRNA in primary neurons and mouse brain. Mol Ther Nucleic Acids. 2015; 4:e266. [PubMed: 26623938]
16. Livak KJ, Schmittgen TD. Analysis of relative gene expression data using real-time quantitative PCR and the 2(−Delta Delta C(T)) Method. Methods. 2001; 25(4):402–408. [PubMed: 11846609]
17. Han IK, Kim MY, Byun HM, Hwang TS, Kim JM, Hwang KW, et al. Enhanced brain targeting efficiency of intranasally administered plasmid DNA: an alternative route for brain gene therapy. J Mol Med. 2007; 85(1):75–83. [PubMed: 17089096]
18. Ross TM, Martinez PM, Renner JC, Thorne RG, Hanson LR, Frey WH 2nd. Intranasal administration of interferon beta bypasses the blood-brain barrier to target the central nervous system and cervical lymph nodes: a non-invasive treatment strategy for multiple sclerosis. J Neuroimmunol. 2004; 151(1–2):66–77. [PubMed: 15145605]
19. Kim ID, Shin JH, Lee HK, Jin YC, Lee JK. Intranasal delivery of HMGB1-binding heptamer peptide confers a robust neuroprotection in the postischemic brain. Neurosci Lett. 2012; 525(2): 179–183. [PubMed: 22877697]
20. Thorne RG, Pronk GJ, Padmanabhan V, Frey WH 2nd. Delivery of insulin-like growth factor-I to the rat brain and spinal cord along olfactory and trigeminal pathways following intranasal administration. Neuroscience. 2004; 127(2):481–496. [PubMed: 15262337]
21. Vaka SR, Sammeta SM, Day LB, Murthy SN. Delivery of nerve growth factor to brain via intranasal administration and enhancement of brain uptake. J Pharm Sci. 2009; 98(10):3640–3646. [PubMed: 19156912]
22. Yang JP, Liu HJ, Cheng SM, Wang ZL, Cheng X, Yu HX, et al. Direct transport of VEGF from the nasal cavity to brain. Neurosci Lett. 2009; 449(2):108–111. [PubMed: 18996442]
23. De Rosa R, Garcia AA, Braschi C, Capsoni S, Maffei L, Berardi N, et al. Intranasal administration of nerve growth factor (NGF) rescues recognition memory deficits in AD11 anti-NGF transgenic mice. Proc Natl Acad Sci U S A. 2005; 102(10):3811–3816. [PubMed: 15728733]

24. Harmon BT, Aly AE, Padegimas L, Sesenoglu-Laird O, Cooper MJ, Waszczak BL. Intranasal administration of plasmid DNA nanoparticles yields successful transfection and expression of a reporter protein in rat brain. Gene Ther. 2014; 21(5):514–521. [PubMed: 24670994]
25. Wang Y, Huang L. A window onto siRNA delivery. Nat Biotech. 2013; 31(7):611–612.
26. Karlsson JO, Kurz T, Flechsig S, Näsström J, Andersson RG. Superior therapeutic index of calmangafodipir in comparison to mangafodipir as a chemotherapy adjunct. Transl Oncol. 2012; 5(6):492–502. [PubMed: 23323161]
27. Discalzi G, Pira E, Herrero Hernandez E, Valentini C, Turbiglio M, Meliga F. Occupational Mn parkinsonism: magnetic resonance imaging and clinical patterns following CaNa2-EDTA chelation. Neurotoxicology. 2000; 21(5):863–866. [PubMed: 11130292]
28. Cersosimo MG, Koller WC. The diagnosis of manganese-induced parkinsonism. Neurotoxicology. 2006; 27(3):340–346. [PubMed: 16325915]
29. Criswell SR, Perlmutter JS, Huang JL, Golchin N, Flores HP, Hobson A, et al. Basal ganglia intensity indices and diffusion weighted imaging in manganese-exposed welders. Occup Environ Med. 2012; 69(6):437–443. [PubMed: 22447645]
30. Kim EA, Cheong HK, Choi DS, Sakong J, Ryoo JW, Park I, et al. Effect of occupational manganese exposure on the central nervous system of welders: 1H magnetic resonance spectroscopy and MRI findings. Neurotoxicology. 2007; 28(2):276–283. [PubMed: 16824604]
31. Roth JA. Homeostatic and toxic mechanisms regulating manganese uptake, retention, and elimination. Biol Res. 2006; 39(1):45–57. [PubMed: 16629164]
32. Barron TF, Devenyi AG, Mamourian AC. Symptomatic manganese neurotoxicity in a patient with chronic liver disease: correlation of clinical symptoms with MRI findings. Pediatr Neurol. 1994; 10(2):145–148. [PubMed: 8024663]
33. Roth JA, Feng L, Walowitz J, Browne RW. Manganese-induced rat pheochromocytoma (PC12) cell death is independent of caspase activation. J Neurosci Res. 2000; 61(2):162–171. [PubMed: 10878589]
34. Sava V, Mosquera D, Song S, Cardozo-Pelaez F, Sanchez-Ramos JR. Effects of melanin and manganese on DNA damage and repair in PC12-derived neurons. Free Radic Biol Med. 2004; 36(9):1144–1154. [PubMed: 15082068]

Appendix A. Supplementary data

Supplementary data related to this article can be found at http://dx.doi.org/10.1016/j.jddst.2017.11.013.

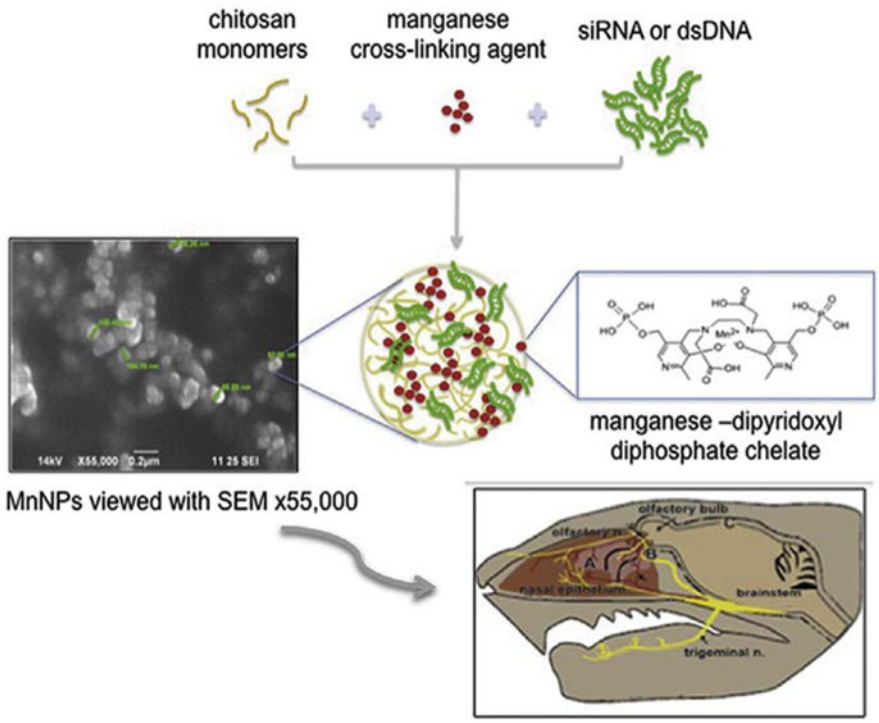

Fig. 1.

Graphical Abstract: Nanoparticles were fabricated of low molecular chitosan electrostatically bound with oligonucleotides by linking its polymer chains with a di-pyridoxyl diphosphate chelate of Mn ion (Mangafodipir). Nanoparticles were administered by intranasal infusion, tracked and visualized in brain by MRI. Biological responses (gene silencing or gene expression) were measured in olfactory bulb, cortex, striatum and hippocampus.

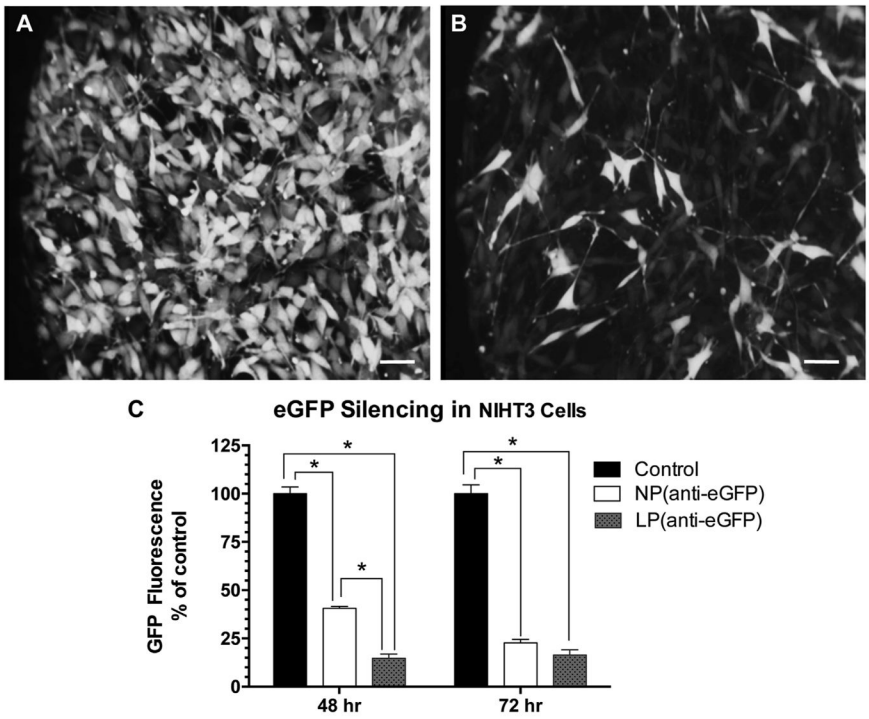

Fig. 2.

In vitro silencing of GFP following incubation of mouse embryonic fibroblast NIH 3T3/GFP cells (Cell Biolabs, San Diego, CA) with mNPs loaded with siRNA against GFP (Stealth RNAi™ siRNA GFP from Invitrogen). (A, B) GFP+ cells before and 48 h after adding NPs (*anti*-GFP siRNA); (C) GFP fluorescence signal measured with plate reader at 520 nM and normalized per 1 mg of protein (n = 8 per treatment). 2-way ANOVA (treatment and time factors) revealed NP and lipofectamine treatments significantly decreased GFP fluorescence at both 48 and 72 h ($p < 0.001$). Treatment factor $F = 5.24$, $p = 0.03$; Time factor $F = 480$; $p < 0.0001$. Asterisk indicates significant difference between NP and lipofectamine at 48 hr but not at 72 hr ($p < 0.05$ Tukey multiple comparisons).

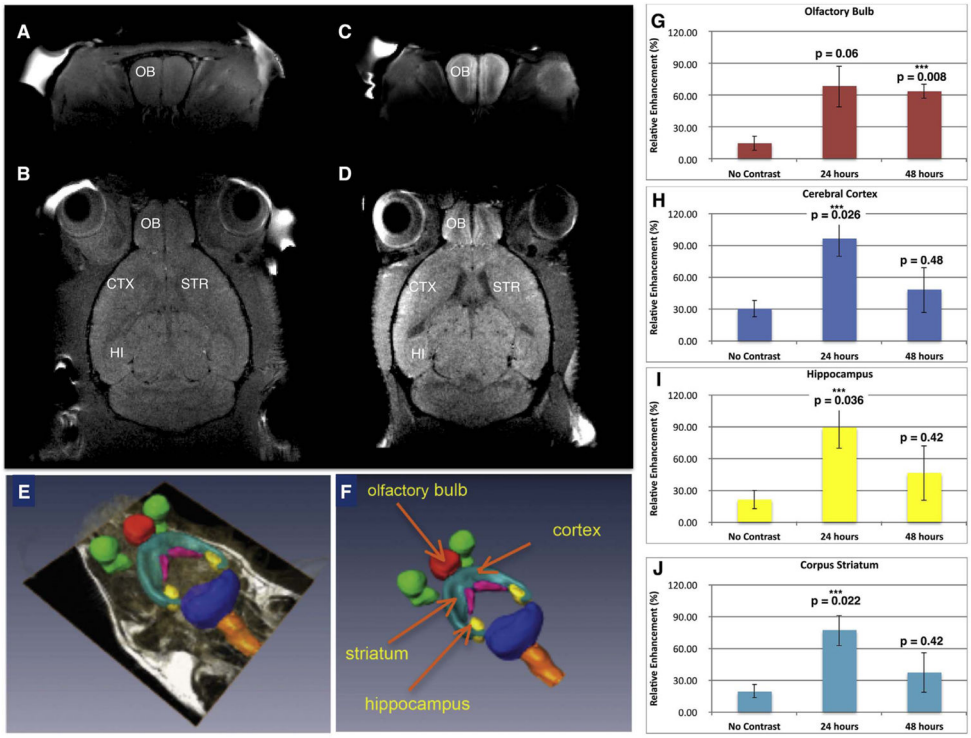

Fig. 3.

Mn-containing NPs were visualized and tracked by MRI. A) Baseline T1-weighted image of coronal section through olfactory bulb and B) baseline horizontal section showing the anatomical regions of interest. C) T_1-weighted MR of mouse 24 h after administration of mNPs showing enhanced Mn signal in coronal section of olfactory bulb, and D) T1-weighted image signal in horizontal section including olfactory bulb, cerebral cortex, striatum and hippocampus. E, F) Parcellation of brain regions (to demarcate brain structures) was performed to quantify Mn signal at 24 and 48 h. G) Olfactory bulb; H) Cerebral Cortex; I) Hippocampus; J) Corpus Striatum. Mean Mn signal (±SEM, n = 3) was increased in all brain regions at 24 and 48 hrs compared to control mice (ie “no contrast”) after intranasal instillation. One-way ANOVA was performed for each brain region using Matlab Statistics Toolbox (Mathworks, Inc.).

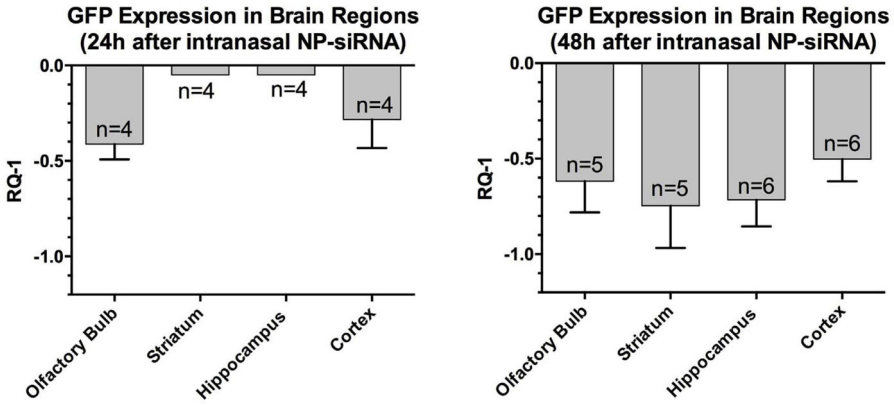

Fig. 4.

Effects on expression of GFP at 24 and 48 hrs after intranasal administration of mNP-*anti*-GFP. Y-axis shows mean ± SEM of GFP mRNA expression expressed RQ-1. A one sample *t*-test comparing mean decrease in RQ-1 in each brain region to zero (no change) at 48 hrs revealed a p value (two tailed) = 0.0012; t = 11.7; df = 3.

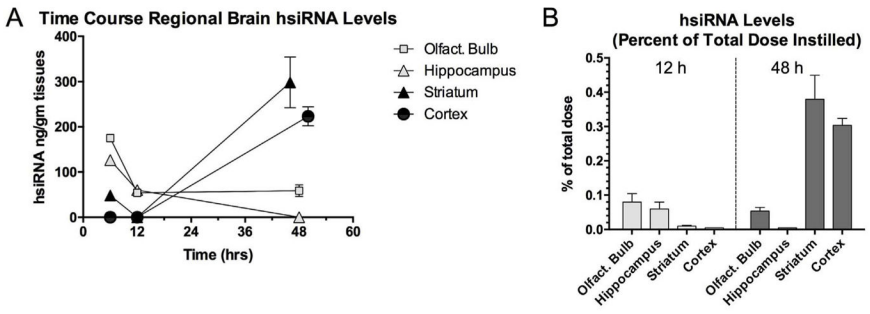

Fig. 5.

Time-course of regional brain distribution of fluorescently-labeled hsiRNA packaged in mNPs instilled intranasally in C57BK6J mice. A) Mean ± SEM (n = 4) concentrations (pg/mg tissue) of hsiRNA in specific brain regions plotted against time after intranasal instillation. Over time the levels of hsiRNA in olfactory bulb and hippocampus decline as levels in cortex and striatum increase; B) Percent of administered dose of hsiRNA in four brain regions after 48 hrs. Y-axis indicates concentration of tissue hsiRNA expressed as percentage of the total administered intranasal dose. Striatum and cerebral cortex accumulated the greatest percentage of the administered dose. Of the total dose of hsiRNA administered intranasally, 0.72% of the dose (estimated by adding percentages of total dose from each region) was located in those regions after 48 hrs.

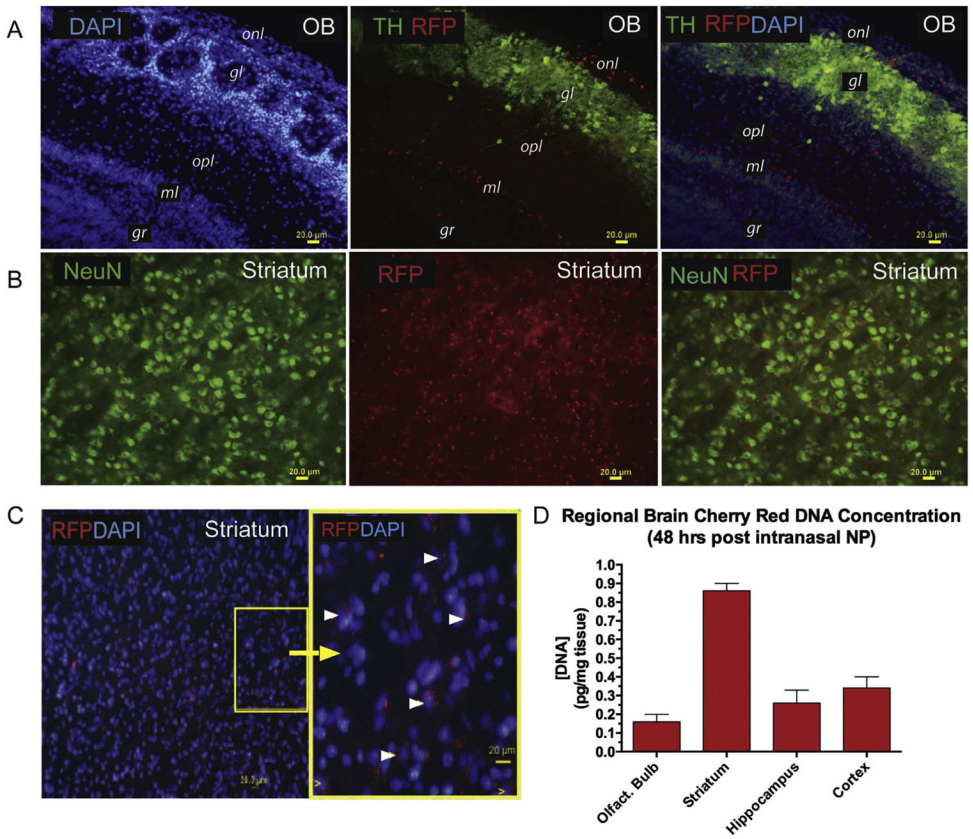

Fig. 6.

RFP expression in mouse brains following intranasal instillation of mNPs containing dsDNA encoding RFP. Mice were euthanized at 24 h for fluorescence histology and at 48 hr for measurement of RFP DNA regional brain concentration.

A) Olfactory bulb. Left panel: Structure of the olfactory bulb is visualized with DAPI staining, which stains all cell nuclei. Middle panel: Tyrosine hydroxylase (TH) immunostaining in green identifies dopaminergic neurons located in the glomerulosa layer. Red identifies cells that express red fluorescent protein (RFP), indicating that the plasmid DNA encapsulated in the manganese-containing nanoparticles is expressed. Right panel: Merged image of DAPI, TH and RFP. onl = olfactory nerve layer; gl = glomerular layer; opl = outer plexiform layer; ml = mitral cell layer; gr = granular cell layer.

B) Corpus striatum. Left panel: neurons immunostained with antibodies against neuron specific nuclear protein (NeuN); Middle panel: RFP expression; right panel: merged image of NeuN and RFP.

C) Ventral striatum. Left panel: DAPI-stained nuclei and RFP expression; Right panel: magnified yellow box from panel on left shows RFP expression in cytoplasm distributed in a perinuclear pattern in many, but not all cells.

D) Regional brain concentrations of RFP DNA was determined at 48 hrs after nasal instillation Mn-nanoparticles containing DNA encoding RFP as described in methods section. Data are expressed as mean and SEM for each brain region (n = 4 mice). Y-axis indicates concentration of DNA (pg/mg tissue). Highest mean concentration of RFP DNA

was observed in striatum with the lowest concentration found in olfactory bulb at this time point.

Table 1

Characterization of mNP used for intranasal delivery of different nucleic acid payloads to the brain.

Payloads	Molecular ratios of mNP constituents			Average Diameter ± Standard Error, nm[a]
	Nucleic acid	Mn chelate	Chitosan	
Stealth *anti*-GFP siRNA	2–2.3	12–14	1	122 ± 15
mCherry RFP plasmid	1	321–365	25–30	140 ± 18
Cy-3-hsiRNA	2–2.5	11–13	1	125 ± 14

[a]Number of replications n = 6.